JOURNAL OF MATERIALS SCIENCE 24 (1989) 3021–3028

Matrix microstructure effect on the abrasion wear resistance of high-chromium white cast iron

S. TURENNE, F. LAVALLÉE, J. MASOUNAVE
Industrial Materials Research Institute, National Research Council Canada, 75 De Mortagne, Boucherville (Quebec) , Canada J4B 6Y4

The two-body abrasion resistance of high-chromium white cast iron was investigated as a function of cast iron microstructure. Different microstructures were obtained by means of heat treatment. The chromium and carbon content were chosen in order to have different matrix microstructures (austenitic, martensitic and ferritic) with the same amount of eutectic carbide (M_7C_3). The results show that the cast iron with an austenitic matrix has the best wear resistance. The good wear resistance of this material is due to strong work hardening of the austenitic matrix resulting in a hardness which exceeds that of other structures. The effect of abrasive paper deterioration on abrasion has also been investigated.

1. Introduction

It is well known that high chromium white cast iron has very good abrasive wear resistance. The use of this material is often encountered in the mining industry where ore has to be ground (crushers, ball mills) or transported (slurry pumps, liner plates) [1–3]. The high chromium white cast iron has good corrosion resistance due to the high concentration of chromium in the matrix and high abrasion resistance due to the presence of eutectic carbides (M_7C_3). These carbides have higher hardness than the austenitic or martensitic matrix. The hardness of the eutectic carbides is also higher than that of quartz which is present in large proportions in a lot of ore types.

The wear resistance is not an intrinsic property of materials, rather it depends on a set of conditions defining a system [4]. As a consequence, the wear resistance is only partially a function of the hardness of a material. The bulk hardness of white cast irons is increased when the amount of carbide, the matrix hardness or both are increased [5]. A lot of studies show that the wear resistance in three-body abrasion [6] and erosion at glancing angles [7] correlates well with the bulk hardness. There is some disagreement when an abrasive harder than the eutectic carbides is used [5]. Also the behaviour of white cast iron is not the same in two- and three-body abrasion [8]. The wear mechanisms involved for the eutectic carbides and the matrix are different and strongly related to experimental conditions. For instance, some studies [8–10] show that under garnet paper abrasion, white cast iron having a martensitic matrix has better wear resistance than white cast iron with an austenitic matrix, while the inverse is the case for alumina or silicon carbide abrasive papers.

The purpose of our study is to investigate the role of the matrix microstructure under severe abrasion. The cast irons to be characterized have the same carbide volume fraction with different matrix microstructures. These specimens were taken from balls used in a ball mill where the abrasion and impact conditions are intense. In this study, only abrasive wear will be considered.

2. Experimental procedures

The high chromium white cast iron balls were supplied by Magotteaux Canada. The compositions and heat treatments were selected so as to obtain different matrix microstructures but with the same carbide volume fraction of nearly 31%. The carbide volume fraction was determined by using Maratray's formula [11]. For the compositions studied, the dendritic austenite formed first and subsequently the eutectic reaction gave M_7C_3-type carbides. The microstructures and the hardness of the white cast iron balls are given in Table I. Cast irons 1A and 3B have a martensitic matrix containing eutectic carbides and small secondary carbides (Fig. 1) formed by solid state diffusion during the cooling. One should note that hardness is constant all along the diameter of the ball. This suggests that the microstructure is nearly the same through the ball. Cast iron 4B has a ferritic matrix obtained by austenizing and quenching at a temperature permitting ferritic transformation. A small

TABLE I

Designation	Matrix Structure	HRC	H_S
1A	Martensitic + secondary carbides	62	982
2A	Austenitic	47	1083
3B	Martensitic + secondary carbides	66.5	920
4B	Ferritic – pearlitic + secondary carbides	32	469

0022–2461/89 $03.00 + .12

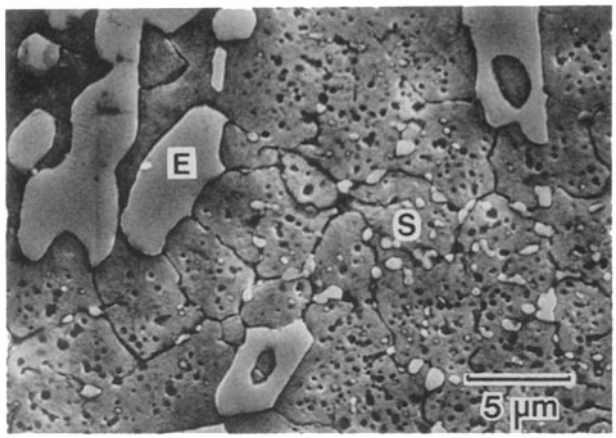

Figure 1 Small secondary carbides (S) in the matrix of martensitic cast iron 1A (E: Eutectic carbides). Etched with 4% nital.

amount of pearlite is also observed. Samples 2A, with austenitic microstructure, were obtained from the same balls as samples 1A. Austenization at 1175°C for two hours results in secondary carbide dissolution in the austenitic matrix. The increase in carbon content of the matrix has the effect of decreasing M_S below room temperature. Rapid quenching to room temperature following the austenization results in an austenitic structure. Due to the heat treatment, the eutectic carbides have a more globular form than those of other cast irons. As a consequence of its heat treatment, cast iron 2A contains no secondary carbides. The microstructures of each cast iron are shown in Fig. 2.

The pin-shaped samples were cut by electro-erosion from balls of 38.1 mm diameter in the as-received conditions. Subsequent machining of the pins resulted in samples with final dimensions of 6.35 mm diameter and 25.4 mm length. One end of each pin was rectified perpendicular to the longitudinal axis in order to maintain the apparent surface constant during abrasion testing. This surface was polished by using 600 grit SiC paper. Before and after each abrasion test, the samples were cleaned in an ultrasonic bath, dried in hot air and weighed. The wear was measured by means of mass loss.

The abrasion tests were made on a machine designed at the Industrial Materials Research Institute. A description of this machine is given elsewhere [12]. The sample is fixed in a holder at the end of a shaft. A rotational speed of 20 r.p.m. is transmitted to the sample which is brought into contact with an abrasive paper belt having a speed of 3.2 m min^{-1}. The two-body abrasion test is carried out with a constant distance travelled on abrasive paper of 6 m under loads of 26.7, 53.3 and 80.0 N. Simultaneously, the sample is displaced laterally in order to guarantee that the sample always travels over fresh paper. The mass loss is well distributed over the surface because the rotation of the sample eliminates the intense wear of the leading edge.

Three different kinds of abrasive paper were used: alumina, garnet and silicon carbide. These were all 100 grit abrasive papers corresponding to an abrasive particle diameter of about 150 μm.

Some microhardness measurements of the matrix

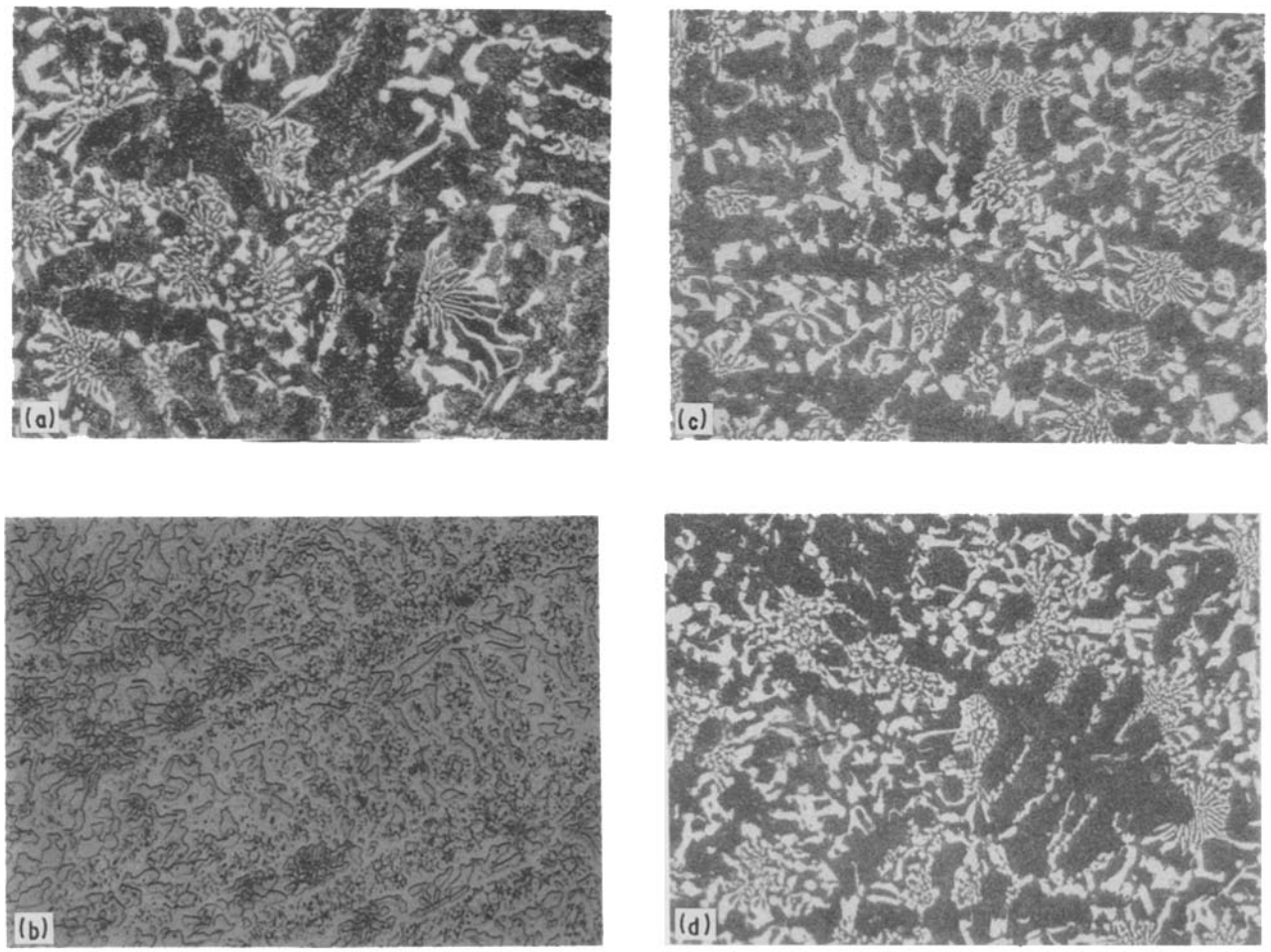

Figure 2 Optical micrograph of cast iron structures. (a) 1A, (b) 2A, (c) 3B and (d) 4B.

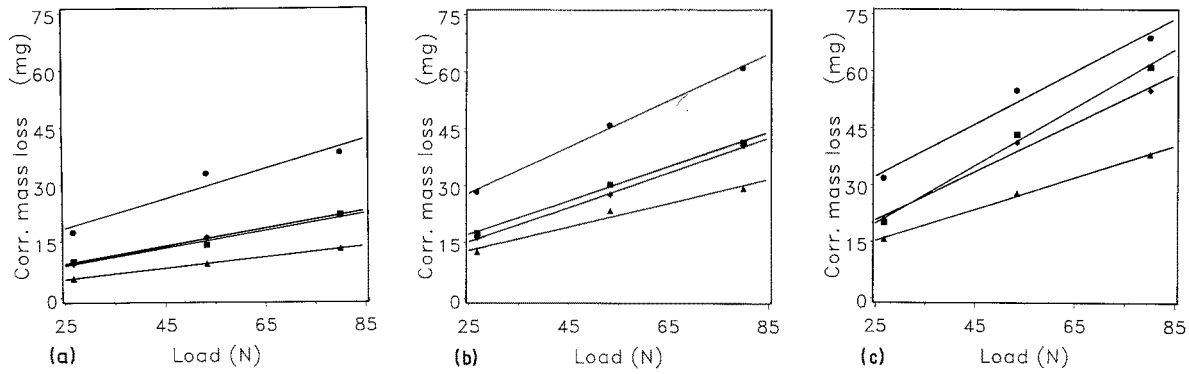

Figure 3 Corrected mass loss plotted against normal load on samples. Comparison of each cast iron for abrasion on (a) garnet, (b) alumina and (c) silicon carbide abrasive paper. (■ 1A, ▲ 2A, ◆ 3B, ● 4B)

were made after the test to determine if structural modifications had occurred. The worn surfaces were lightly polished with 600 grit SiC paper in order to obtain flat surfaces without destroying the deformed layer related to wear. The polishing scratches are much smaller than the ones due to wear. A light etching with 4% nital reveals the carbide and matrix phases. The microhardness measurements were made between the carbides and the penetration marks were 6 to 10 times smaller than the distance between the carbides. The measured Vickers hardnesses H_s (50 gf) of matrices after the testing are reported in Table I.

3. Abrasivity of paper belts

It is necessary to introduce a correction factor to normalize the results of mass losses due to the difference in the severity of abrasion from one paper belt to another for the same type of abrasive. Thus, the relative abrasivity coefficient η_i for a given paper belt is defined as the ratio of $\bar{W}$ over W_i where $\bar{W}$ is the average mass loss of a standard pin using a number of different abrasive paper belts of the same type while applying the same experimental conditions and W_i is the mass loss of a standard pin for the abrasive belt i.

Each paper belt can be used for testing three pins. Since one standard is used to determine η_i, only two actual samples are tested per belt. Any variations of abrasivity between different locations on the same belt were shown to be negligible. The standard material used in this study is a low alloyed steel with a martensitic microstructure. The corrected mass loss of a sample will then be

$$W_{corr} = \eta_i W_{mes}$$

where W_{mes} is the measured mass loss of the sample and W_{corr} is the corrected mass loss.

$\bar{W}$ was calculated from a set of 15 measurements of mass loss for each paper type. The minimum and maximum values of η_i were respectively 0.85 and 1.2.

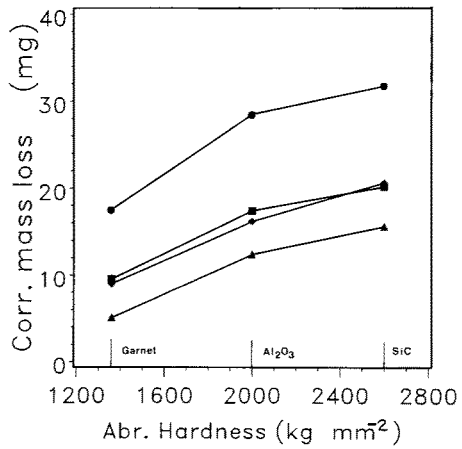

Figure 4 Corrected mass loss plotted against abrasive hardness for a load of 26.7 N. (■ 1A, ▲ 2A, ◆ 3B, ● 4B)

4. Results

4.1. Influence of the load

For each test condition, two samples were tested and the mean of the two measures reported as the corrected mass loss (Fig. 3). It is clearly demonstrated that relative mass loss increases with the load. Austenitic white cast iron (2A) shows the best wear resistance under all load and abrasive hardness conditions. The wear rate of cast iron 2A as indicated by the slope of the straight line is slightly lower than the wear rate of the other cast irons. Martensitic white cast irons 1A and 3B show almost the same behaviour within the experimental error. Some experiments were made with a load of 111 N; in these cases, the result was usually a torn abrasive paper. Within the range of loads studied, the wear resistance of the different white cast irons investigated are of the same order of magnitude for garnet, alumina and silicon carbide abrasive paper. The increasing order of abrasive wear resistance for the various matrices is: ferritic (4B), martensitic (1A and 3B) and austenitic matrices (2A).

4.2. Influence of abrasive and material hardness

The mass losses of the samples studied as a function of abrasive hardness are plotted on the graph shown in Fig. 4. The values of hardness for the abrasives employed were taken from references [13, 14]. The abrasive paper belts were observed under the scanning electron microscope before and after the tests. The deterioration of abrasive paper differs for the different types of abrasive. As an example, Fig. 5 illustrates the appearance of SiC abrasive paper before and after testing. There are two important features to mention: the efficiency of the binder and the fracture of the abrasive particles. Sometimes the binder is already cracked before the abrasion test; this results in a more rapid degradation of abrasive paper. The morphology of garnet abrasive particles is different from the

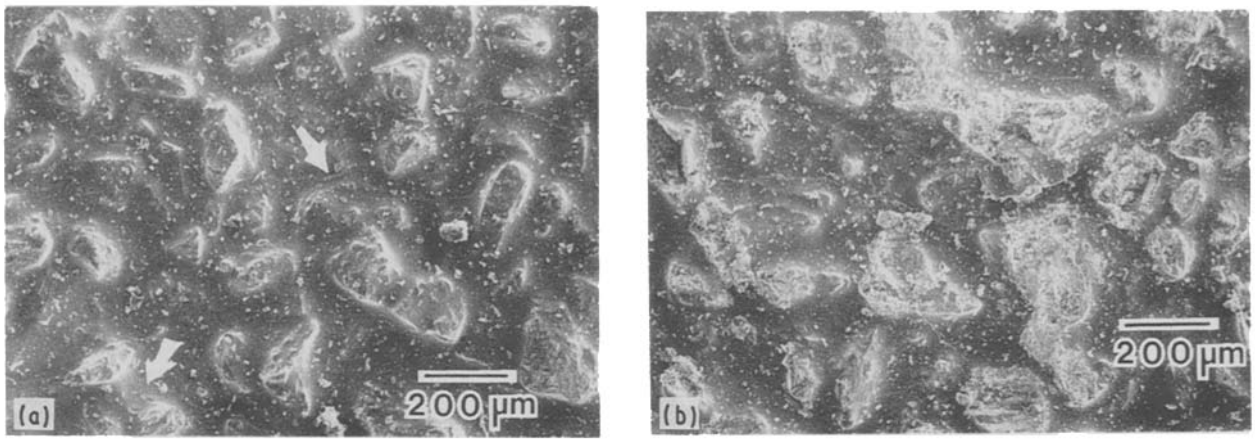

Figure 5 Silicon carbide abrasive paper (a) before and (b) after the test under a load of 26.7 N. Arrows indicate the cracked binder before the test.

morphlogy of alumina or silicon carbide. Moreover, the quantity of binder is greater for alumina and silicon carbide papers than for garnet paper. The fracture of garnet particles yields large abrasive particles with angular edges (Fig. 6) which are easily removed from the paper leading to three-body abrasion. The Al_2O_3 and SiC particles are broken into a large number of small particles (Fig. 7). The flattening of the three types of abrasive particles was also observed. On the flat surfaces formed, cast iron deposits can be detected, as shown in Fig. 8.

The hardness of the material undergoing wear testing is a preponderant parameter. The hardness values H_S (presented in Table I) are those prevailing at the moment of testing. The considered hardness is then taken in the matrix after the tests following the method described previously. The wear resistance defined as the inverse of mass loss for a 6 m length is plotted in Fig. 9a as a function of the ratio of the matrix hardness to the abrasive hardness. The well known rule stating that the hardest material has the best wear resistance is verified in our experiment since the amount and hardness of the eutectic carbide phase M_7C_3 is the same in all white cast iron specimens. The wear resistance variation is almost the same for different types of abrasive paper employed as shown in Fig. 9b. For a small increase in hardness from martensitic to work hardened austenitic cast iron, there is a large increase in wear resistance. Fig. 9c illustrates the wear resistance as a function of the ratio of HRC bulk hardness (converted in Vickers hardness unit) to the abrasive hardness.

4.3. SEM observations of worn surfaces

The wear mechanisms identified on the worn surfaces are microcutting and ploughing. The ploughing mechanism is observed from the occurrence of plastically deformed lips on the side of wear grooves (Fig. 10). The intense stress at the tip of abrasive particles results in plastic strain in the surface layer even in the case of a hard martensitic matrix, as shown in Fig. 11. Typical

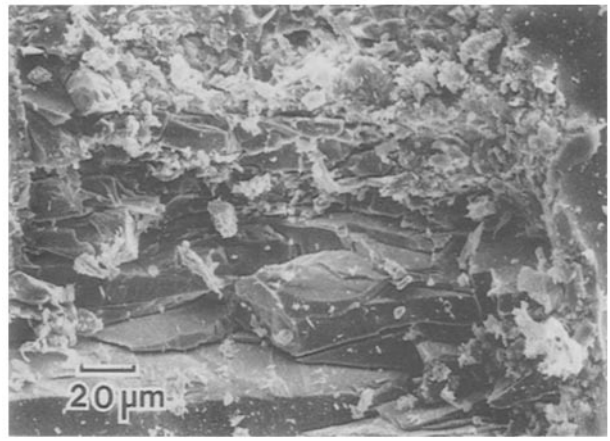

Figure 7 Thin platelets and small particles result from the fracture of SiC particles.

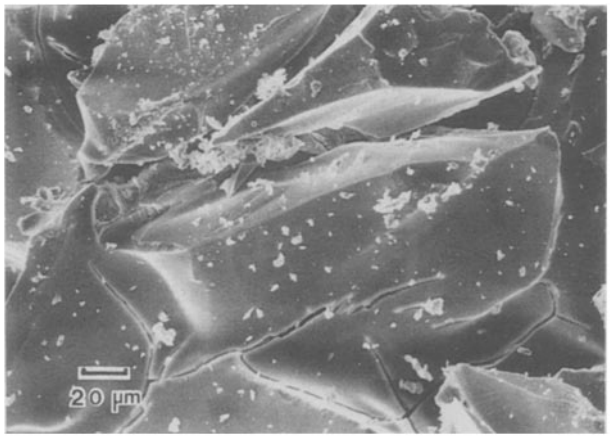

Figure 6 Breakdown of garnet particle yielding large and angular abrasive particles.

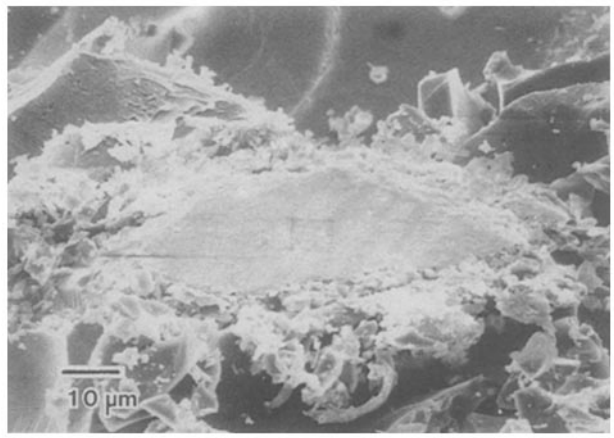

Figure 8 Presence of cast iron deposits on the surface of the garnet particle flattened during the test.

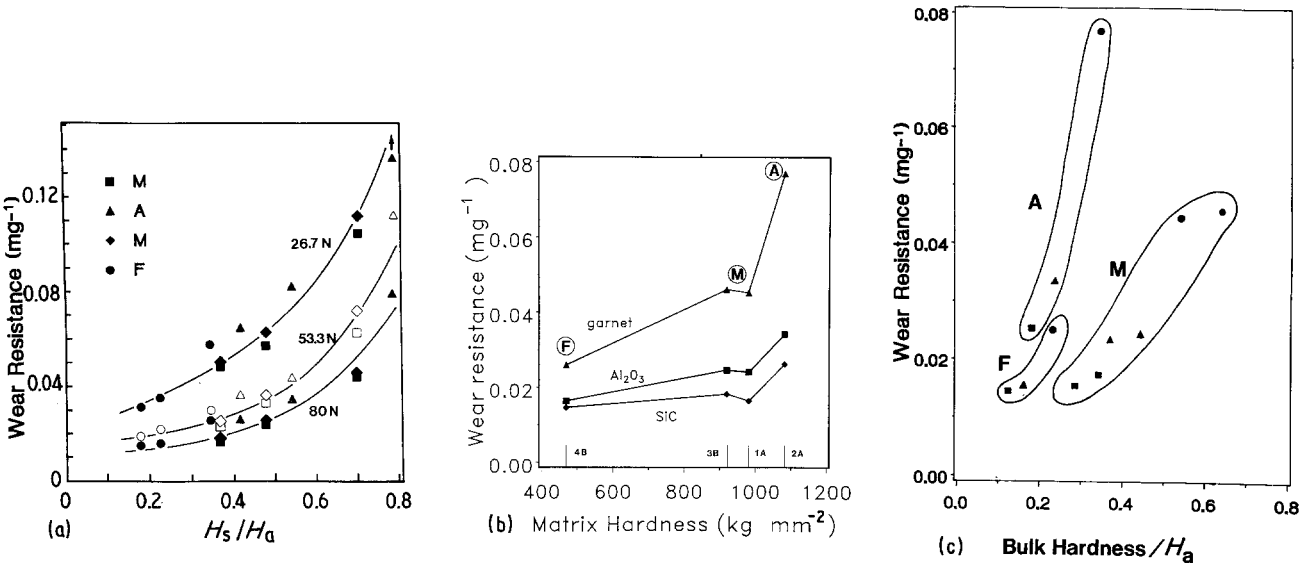

Figure 9 (a) Wear resistance plotted against the ratio of the matrix hardness to the abrasive hardness, (b) wear resistance plotted against matrix hardness measured after the test. A: austenitic, M: martensitic, F: ferritic, (load 80 N, abrasion distance 6 m), (c) Wear resistance plotted against the ratio of the bulk hardness to the abrasive hardness (load 80 N). ■ SiC, ▲ Al_2O_3, ● garnet.

worn surfaces of each cast iron for the same load and type of abrasive are illustrated in Fig. 12. When looking at these micrographs, it is possible to distinguish the ferritic cast iron from the martensitic or austenitic cast irons by observing the differences in groove depths and groove lip dimensions. Austenitic and martensitic cast irons have almost the same worn surface characteristics.

Prior to observations under the scanning electron microscope, some samples were lightly etched to observe the wear mechanism of carbides and the role of matrix–carbide interface. Fig. 13 shows that there is no evidence of discontinuity of wear grooves at the matrix–carbide interface. The grooves in the carbides look smooth and no tearing or lip formation occurs like in the matrix grooves (Fig. 10). Some samples were cut perpendicularly to the test surface in order to observe the deformation of material under the surface. Fig. 14a illustrates that the carbides are broken at a depth up to 10 μm for the ferritic cast iron. Moreover, Fig. 14a shows decohesion which is usually an indication of large plastic deformation. The large plastic deformation of the matrix would be the most likely cause of the breakage of carbides. Carbide fracture was rarely observed for martensitic (Fig. 14b) and austenitic cast irons.

5. Discussion

In agreement with Archard's paper [15], the wear losses observed in our study are about proportional to the load. This relationship exists because the penetration depth increases with the load. For the same reason, the hardness of pure materials correlates well with wear resistance [16]. The presence of a second phase modifies the wear behaviour of materials generally in a different way to the one predicted by the linear rule of mixtures [5].

The wear of white cast iron with a martensitic matrix occurs by microcutting and ploughing. During the abrasion test large deformations within the surface layer produce heat [17, 18] which tends to improve the toughness and the ductility of a brittle material. The depth of this surface tempering corresponds to the thickness of the plastically deformed layer [18]. This thickness depends on the type of abrasive and the bulk

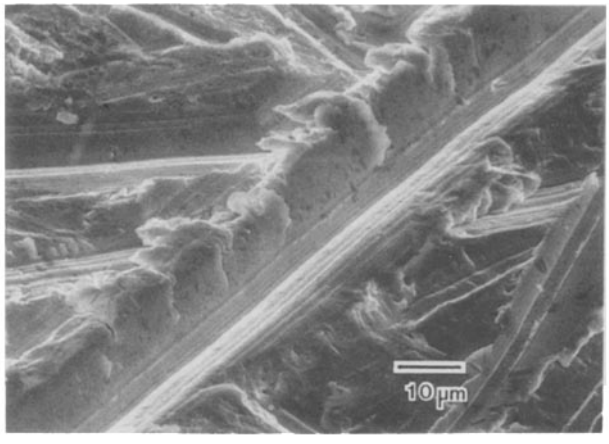

Figure 10 Lips adjacent to wear grooves produced by ploughing. Cast iron 3B tested under a load of 80 N with SiC abrasive paper.

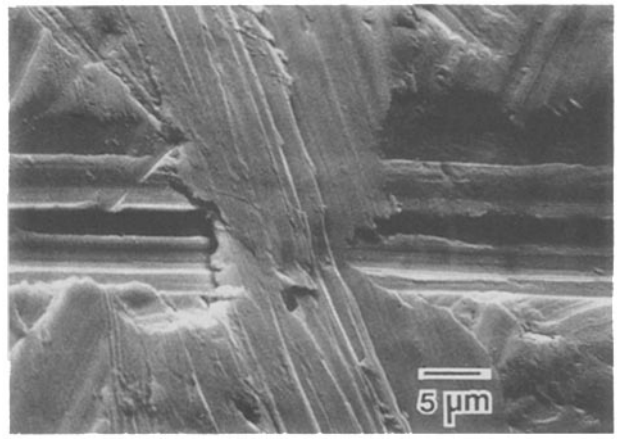

Figure 11 Important plastic deformation occurs at the intersection of two wear grooves. Cast iron 1A tested under a load of 80 N with SiC abrasive paper.

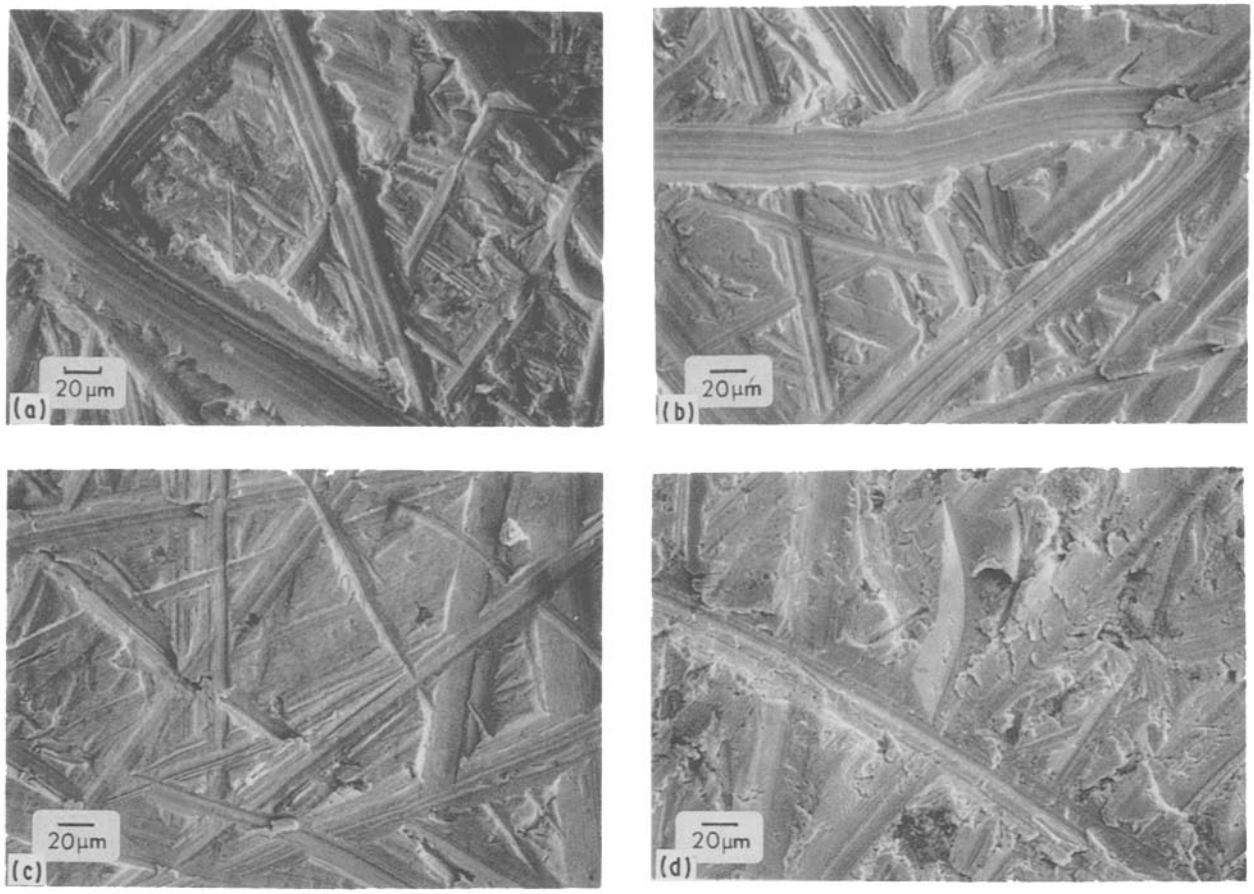

Figure 12 Typical worn surfaces of cast iron (a) 1A, (b) 3B, (c) 2A and (d) 4B tested under a normal load of 53.3 N with SiC abrasive paper.

hardness of the material. The hard region under the surface layer limits the penetration of abrasive particles and only a small fraction of eutectic carbides are abraded during the test. As shown in Fig. 12, the lips of the grooves in austenitic white cast iron are very small if not totally absent as compared to the martensitic or ferritic matrix. The higher microhardness after the tests is a good indication that strong work hardening and maybe martensitic transformation occurs within the surface layer. Samuels [17] mentions that it is difficult to observe evidence of martensitic transformation in the surface layer. As the high hardness of the work hardened surface is combined with a certain amount of ductility of the austenitic matrix, the wear losses associated with the austenitic matrix are smaller than the wear losses associated with the martensitic matrix. Ductility increases the amount of ploughing; pure ploughing is known not to produce material losses [19]. The very small size of the lips formed on the austenitic white cast iron is due to the weak penetration of abrasive particles in work hardened austenitic matrix. Also the small lips formed obstruct further material displacements caused by the passage of other abrasive particles. The rotation of the sample facilitates the removal of the lips. The lip material is more easily removed when abrasive particles arrive almost perpendicular to the grooves. The low hardness of white cast iron with a ferritic matrix is mostly responsible for the higher wear losses. During the microcutting and ploughing of this soft matrix, another wear mechanism is involved. The micrograph in Fig. 12d illustrates the lip and groove tearing of ferritic cast iron. The microcracks created by this mechanism facilitate material removal during the subsequent passage of abrasive particles. The low hardness of ferritic cast iron after testing, as can be seen in Table I, indicates that work hardening is not significant. This also contributes to high wear losses associated with deep wear grooves.

The eutectic carbides in white cast irons play an important role. The hardness of these carbides is about 1300 to 1800 HV [8, 14] and is situated between the hardnesses of garnet and alumina. It is one of the reasons why the curves of corrected mass loss against abrasive hardness (Fig. 4) are not linear. Even though garnet is slightly softer than M_7C_3 carbides, grooves in carbides are formed indicating that the angularity of

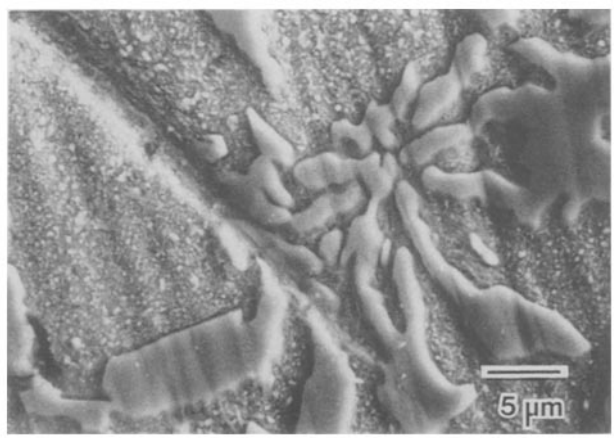

Figure 13 Abrasion groove through eutectic carbides on cast iron 3B tested for a load of 80 N with garnet abrasive paper.

abrasive particles is a part of the wear system that also has to be taken into consideration. The ratio of M_7C_3 carbide hardness over garnet hardness gives values from 0.95 to 1.32 which are slightly over 0.8 corresponding to the value defined by Richardson [20] as the limit of ability of abrasive particles to produce grooves on carbides. From our observations, the abrasive particles cut M_7C_3 carbides at the same rate as matrix material. This is deduced from the absence of protruding carbides on the surface (Fig. 13) and the constant size of the grooves from the matrix to the bigger carbides (5 to 20 μm). A major part of the wear resistance of the white cast irons is due to the matrix hardness during abrasion. The high work hardening ability of the austenitic matrix brings the surface hardness high enough to result in a wear resistance surpassing the one of the martensitic cast irons.

To compare the different cast irons, it is necessary to consider the surface hardness instead of the bulk hardness. The bulk hardness does not take into account the work hardening of the matrix which occurs during the wear test. Fig. 9c illustrates that a relation exists between wear resistance and bulk hardness of cast irons only when looking at cast irons with the same matrix. The method employed to measure the surface hardness seems to be good because the curves in Fig. 9a are similar for the three loads suggesting that the depth of the penetration marks is contained entirely in the work hardened layer.

The wear resistance as a function of matrix hardness (Fig. 9b) is also strongly influenced by the stress distribution at the interface between matrix and carbides [5]. By varying the ratio of the hardness of the matrix over the hardness of the carbides, different points of stress concentration may result in different material displacements and wear losses. The deformation mismatch between the ferritic matrix and eutectic carbides produces decohesion at matrix–carbide interfaces (Fig. 14) [13] resulting in formation of microcracks which look like tearing in the grooves (Fig. 12d).

There are other testing parameters besides the hardness of the abrasive that play a role. One also should look at the effect of abrasive binder which is different in our case for each type of abrasive. The thickness and resistance of the binder have a strong influence on stress concentration in the abrasive particles. The use of larger amounts of binder for SiC paper results in particles fracturing at many points yielding small fragments (Fig. 7). For garnet, the quantity of binder is smaller and original abrasive particles break into fewer and bigger fragments (Fig. 6). Also, the smaller amount of binder for the garnet abrasive paper results in protruding particles lightly anchored at their bases compared to SiC particles which are well attached to the paper. In both situations, free particles lead to three-body abrasion. The behaviour of materials under two- and three-body abrasion conditions can differ greatly and this dual wear mechanism can be reduced by having a sample pin diameter small enough to eliminate three-body abrasion.

5. Conclusions

The results of the two-body abrasion tests and observations under the scanning electron microscope suggest the following conclusions.

- Microcutting and ploughing are the prevailing wear mechanisms for all the cast irons observed. The proportion of ploughing increases with the ductility of the matrix. For the ferritic matrix, tearing in grooves results in surface deterioration that increases the mass loss for a given experimental condition.
- Decohesion at ferritic matrix–carbide interface and carbide fracture under the worn surface result in high wear rate compared to other matrix microstructures investigated.
- The groove depth is well correlated with mass losses due to abrasive wear.
- Due to work hardening during testing, the austenitic matrix shows better wear resistance than the martensitic matrix in spite of the fact that the initial hardness of the austenitic matrix is lower than the hardness of martensitic matrix.
- The wear rate of the eutectic carbides and the matrix are the same for a given cast iron microstructure.
- In the interpretation of the results of two-body abrasion test, the different properties of the binder of the abrasive papers have to be considered.

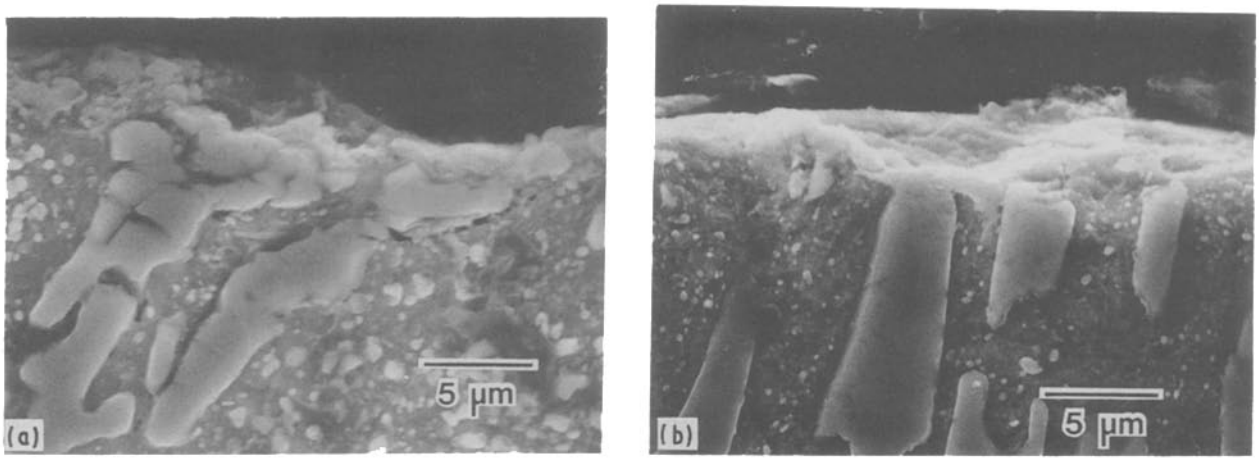

Figure 14 Views perpendicular to the worn surface of samples (a) 4B and (b) 3B tested under a normal load of 80 N with Al_2O_3 abrasive paper.

Acknowledgements

The authors are indebted to Gilles Huard for helpful discussions. Thanks are due to D. Simard and M. Thibodeau for the technical assistance. We gratefully acknowledge Magotteaux Canada for the cast iron balls supplied.

References

1. H. L. ARNSON, J. L. PARKS and D. R. LARSEN, in Proceedings of AIME Intermountain Minerals Conference, Vail, Colorado, August 1982, edited by R. Q. Barr, D. V. Doane and K. H. Miska (Climax Molybdenum Co., Ann Arbor, 1982) p. 25.
2. J. S. CRISI, *Chem. Eng.* **88** (1981) 127.
3. G. F. TRUSSCOTT, in Hydrotransport 6, Canterbury, U.K., September 24–25, 1979, BHRA Fluid Engineering, Chap. 7.
4. H. CZICHOS, in "Tribology, a systems approach", Tribology series 1 (Elsevier, Amsterdam, 1978), p. 14–23.
5. K.-H. ZUM GAHR, in "Microstructure and Wear of Materials", Tribology series 10 (Elsevier, Amsterdam, 1987) p. 132–350.
6. A. MISRA and I. FINNIE, in Proceedings of International Conference on Wear of Materials, San Francisco, California, March 30–April 1 1981, edited by S. K. Rhee, A. W. Ruff and K. C. Ludema (ASME, New York, 1981) p. 426.
7. I. FINNIE, J. WOLAK and Y. H. KABIL, *J. Mater. Sci.* **2** (1967) 682.
8. K.-H. ZUM GAHR and G. T. ELDIS, *Wear* **64** (1980) 175.
9. J. D. WATSON, P. J. MUTTON and I. R. SARE, *Met. Forum* **3** (1980) 74.
10. R. B. GUNDLACH and J. L. PARKS, *Wear* **46** (1978) 97.
11. F. MARATRAY, *AFS Trans.* **79** (1971) 121.
12. Y. THÉRIAULT, Internal report no. 86-204-457, National Research Council Canada, Industrial Materials Research Institute, Boucherville, Quebec, 1986.
13. E. BLANK and E. LUCHSINGER, *Wear* **117** (1987) 289.
14. J. XING, W. LU and X. WANG, in Proceedings of International Conference on Wear of Materials, Reston, Virginia, April 11–14 1983, edited by K. C. Ludema (ASME, New York, 1983) p. 45.
15. J. F. ARCHARD, *J. Appl. Phys.* **24** (1953) 981.
16. A. MISRA and I. FINNIE, *Wear* **68** (1981) 33.
17. L. E. SAMUELS, in "Metallographic Polishing by Mechanical Methods" (ASM, Metals Park, 1982), p. 87–140.
18. G. SUNDARARAJAN, *Wear* **117** (1987) 1.
19. M. M. KHRUSCHOV and M. A. BABICHEV, in "Research on the Wear of Metals" (National Engineering Laboratory Translations, Glasgow, 1960), Chapter 18.
20. R. C. D. RICHARDSON, *Wear* **11** (1968) 245.

Received 9 February
and accepted 13 June 1988